A high repetition rate, picosecond hard xray system, and its application to time resolved xray diffraction

T. Anderson, I. V. Tomov, and P. M. Rentzepis

Citation: The Journal of Chemical Physics **99**, 869 (1993); doi: 10.1063/1.465350
View online: http://dx.doi.org/10.1063/1.465350
View Table of Contents: http://scitation.aip.org/content/aip/journal/jcp/99/2?ver=pdfcov
Published by the AIP Publishing

A high repetition rate, picosecond hard x-ray system, and its application to time-resolved x-ray diffraction

T. Anderson, I. V. Tomov, and P. M. Rentzepis[a)]
Department of Chemistry, University of California, Irvine, California 92717

(Received 5 February 1993; accepted 7 April 1993)

A new technique for generation of hard x-ray picosecond pulses is presented. Excitation of a x-ray diode with 10 ps ultraviolet light pulses produces characteristic x-ray pulses with duration in the range of 10–100 ps at a repetition rate of 300 Hz. The x-ray pulses are synchronized with picosecond accuracy to the optical pulses of the laser system as well to other ultrafast phenomena. Results of picosecond time-resolved x-ray diffraction are reported.

I. INTRODUCTION

X-ray diffraction is a well-established field which provides the most detailed information on the molecular and crystal structure of materials. However, the structure of the fast intermediate states and transient species produced during the interaction of materials with short laser pulses or other ultrafast phenomena have been studied in a limited manner due to lack of short x-ray pulses with proper synchronization capability.

A considerable amount of ultrafast spectroscopy has been performed by means of picosecond and subpicosecond laser techniques. However, ultrafast optical spectroscopy is inherently incapable of providing the detailed information about material structures that can be obtained with x-ray diffraction methods.

X-ray pulses have been generated for several decades and pulsed x-ray sources have been also used to study the change in structure under various conditions.[1–6] Lately, synchrotrons have been employed to generate short x-ray pulses for time-resolved x-ray experiments.[4–6] Synchrotron sources provide high intensity, tunable, and highly collimated x-ray pulses with duration 100–200 ps, but are difficult to synchronize to external sources to an accuracy better than a few nanoseconds. X rays produced by laser induced plasma provide another means for the generation of incoherent and coherent short pulse radiation, but most of the studies are confined to the soft x-ray region.[7] The conventional x-ray tube also has been modified to emit pulses in the millisecond range and flash x-ray techniques are capable of producing nanosecond pulses.[1,2]

These devices which generate short x-ray pulses may be use in time-resolved x-ray diffraction research in areas such as lattice deformation by laser induced heating,[5,8] surface calorimetry,[9] impact induced fast reactions processes,[10] solid state decomposition, and explosion of energetic materials.[11] Each of the above techniques has advantages and disadvantages over the others depending on the specific application. For time-resolved studies such as picosecond x-ray diffraction, a narrow linewidth is required; sources with high flux of the characteristic x-ray radiation are preferred over other sources which generate x-rays with a broader spectrum. In order to achieve time resolution on the picosecond scale in pump–probe type experiments, picosecond synchronization between the pump and probe sources is essential.

In this paper we report the details of a new technique for the generation of picosecond hard x-ray pulses, in the range 1–70 keV, at a high repetition rate and capable of accurate synchronization to other ultrafast sources. The basic idea revolves around the replacement of the cathode in a conventional x-ray diode with photocathode excited by picosecond optical pulses.[12]

II. PULSED OPERATION OF THE X-RAY DIODE

Conventional x-ray diodes operate using thermionic emission as the electron source and therefore have long response times. Replacement of the thermal emitter with a photocathode excited by short laser pulses allows for picosecond x-ray pulses to be easily generated.[12] Photoemission is known to take place on a subpicosecond time scale and electron bunches are produced on the photocathode surface with the same duration as the laser pulse. The operational wavelength of the x-ray diode is otherwise similar to a conventional tube and determined only by the anode material, regardless of the process used in the electron production. The analysis of a space-charge limited, photoexcited diode presented by Girardeau-Montaut and Girardeau-Montaut is used in order to evaluate the performance of the photoexcited x-ray diode.[13,14]

Consider a planar x-ray diode consisting of flat photocathode and flat anode separated by a fixed distance in a vacuum (Fig. 1). Metallic photocathodes are preferable for pulsed x-ray diodes for the following reasons. Although semiconductors and alkali-metal composites possess much greater quantum efficiency (2–3 orders of magnitude) relative to pure metal cathodes, the lower damage threshold, lower peak currents, and limited lifetime makes semiconductors and alkali-metal composites unsuitable for intense laser-driven photoemission applications.[12,15] Additionally, the composite photocathodes demand pressure below 10^{-9} Torr, while pure metal photocathodes required little preparation and a modest vacuum [below 10^{-6} Torr], and allow for very high current densities with virtually unlimited lifetime and easy refurbishment through simple repolishing for reuse. The main disadvantage of a metallic photocathode is its low quantum efficiency and high work function

a)To whom all correspondence should be directed at the above address.

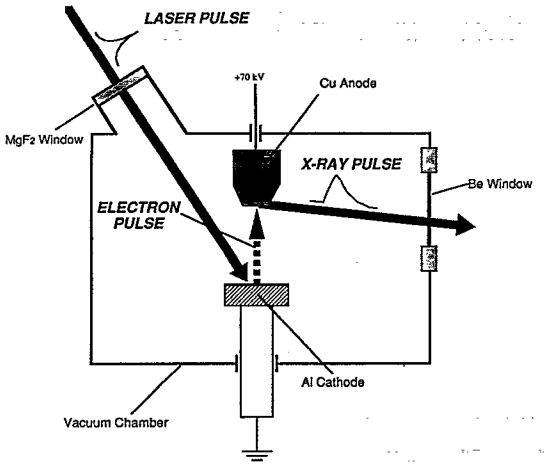

FIG. 1. Schematic diagram of a planar x-ray diode.

which require intense ultraviolet light (UV) for photoemission. Recently, new results have been reported regarding the choice of metals for laser driven metal photocathodes.[15,16]

In a plane diode, the total charge per unit electrode area traveling from cathode to anode through the free space and the electric circuit is

$$q_t(t)=q_c(t)+q_i(t),$$

where q_c is the capacitive charge component per unit area and q_i is the induced charge resulting from electron motion.[13] Before the cathode is illuminated there is no current in the circuit and therefore $q_i=0$. The charge immediately available is the capacitive charge which is of purely static origin. If the applied voltage between electrodes is V, the available charge is

$$q_c=C_sV,$$

where C_s is the diode capacity per unit area. For a plane diode, $C_s=\epsilon_0/d$, where d is the anode–cathode separation and ϵ_0 is the free space permittivity. The particular diode geometry of interest involves anode–cathode distances of 5–15 mm, and applied dc voltage up to 100 kV. The effects related to field emission are negligible and the field strengths are well below the vacuum breakdown threshold.

With such diode geometry and excitation by picosecond light pulses the diode is said to operate in the transient or pulsed mode. In the transient regime, the duration of the electron pulse (t_p), traveling from the cathode to the anode, is shorter than the transit time of the electrons between electrodes. The transit time of nonrelativistic electrons across the diode gap is given by

$$t_t=1.5(2m/e)^{1/2}d/V^{1/2},$$

where e and m are the charge and mass of the electron, respectively.[13]

When all the available capacitive charge q_c has been emitted, the intensity of the electric field at the cathode goes to zero due to charge screening. Any additional photon flux produces electrons at the surface in a roughly zero field environment that mostly results in excess electrons returning to the cathode. Thus when the cathode is illuminated by an intense short light pulse, only the capacitive charge q_c can be extracted. If the time between successive light pulses striking the cathode is longer than the transit time t_t, then only one electron pulse is present in the gap of the diode at a time and the induced charge density is therefore zero. The maximum peak current density is then

$$J_M=q_c/t_p,$$

and is directly related to the light pulse duration t_p. It is a fair assumption that the electron pulse formed at the cathode surface by photoemission initially possesses the same duration as the incident picosecond laser pulses. However, space-charge interaction within the electron pulse during propagation between cathode and anode can result in significant temporal and spatial dispersion, depending on the initial current density of the photoelectron burst. Coulomb repulsion between the electrons inside the pulse is primarily responsible for a longer temporal duration and wider spatial distribution of the electron pulse at the anode.

The duration t_x of the x-ray pulse generated by electron impact on the anode is assumed to be equal to the duration of the electron pulse at the anode, $t_a=t_x$. The spatial distribution of the x rays on the anode surface is largely determined by the final distribution of the electrons at the anode. Computer simulations of the temporal dispersion of short electron pulses traveling across a diode have been reported previously.[14]

It is interesting to compare the transient and steady-state (cw) regimes of operation for this class of devices. When the optical pulse (and therefore the initial electron pulse) duration is greater than the transit time of the electrons across the diode gap, then the electron pulse spans the gap to form a conducting path and the diode operates in the cw mode. The space-charge limited current density in the diode is then governed by the well-known Langmuir–Child equation:

$$J_L=\epsilon_0(32e/81m)^{1/2}V^{3/2}/d^2.$$

Therefore, the transient mode of operation of the diode allows for much higher peak current densities that scales approximately as the ratio of the transit time to the pulse duration:[13]

$$J_M\sim J_Lt_t/t_p.$$

Consequently, one may also expect higher peak x-ray intensities in the pulsed mode of operation.

Narrow linewidth characteristic x-ray radiation is preferable for application to time-resolved diffraction measurements. In the present experiment a copper anode is used to produce K_α radiation with $\lambda=1.54$ Å and $\Delta\lambda/\lambda=2.9\times10^{-4}$. The efficiency of production of characteristic K_α radiation from thick targets of pure elements is well documented.[17,18] Using data for 70 keV electrons, the total K_α photons per electron per unit solid angle is 1.2×10^{-3}.

In this x-ray diode, a polished aluminum disk was used for photoemission. The observed quantum efficiency of Al for 193 nm radiation is 4.65×10^{-4} as measured by the

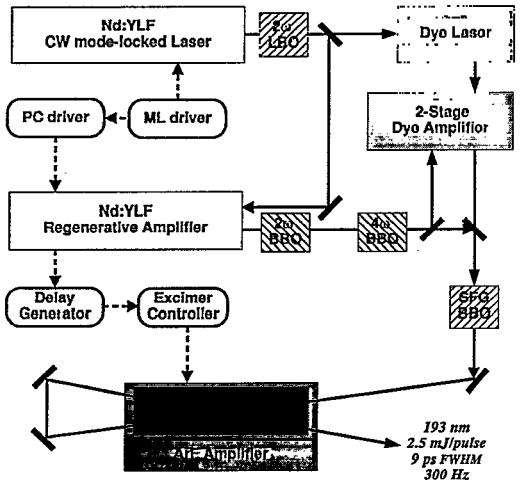

FIG. 2. High repetition rate laser system for generation and amplification of picosecond pulses at 193 nm.

procedure reported in previous work.[16] From the above expression for capacitive charge with a 1 cm anode–cathode separation and an applied voltage of 70 kV, the maximum available charge per pulse per mm^2 equals 4.9×10^{-11} C. This amount of charge will produce 3.7×10^5 Cu K_α photons per pulse per unit solid angle. Accounting for the quantum efficiency of the Al cathode, 67 μJ/cm^2 per pulse of UV radiation at 193 nm is required to extract available charge. At 300 Hz, this corresponds to 20 mW/cm^2 average power density.

III. GENERATION OF INTENSE 193 NM PICOSECOND PULSES

In order to meet the above requirements for the UV pump source that drives the x-ray diode, a high power picosecond laser system based on an ArF excimer amplifier has been developed that generates UV pulses with duration shorter than 10 ps, and pulse energy up to 2.5 mJ at a repetition rate of 300 Hz. The experimental system is shown in Fig. 2. A detailed description of the system is presented in Ref. 19 and therefore only a brief outline will be presented here.

The master oscillator is a cw mode-locked Nd:YLF laser generating 1053 nm pulses with 50 ps duration at 76 MHz and average power of 13 W. Its output is up-converted in a lithium borate (LBO), crystal to generate 2 W of 527 nm radiation for synchronous pumping of a single jet dye laser. The pulse duration of the dye laser is 5 ps and its average output power is 200 mW at 724 nm. Part of the remaining unconverted 1053 nm radiation from the LBO crystal is used to seed a Nd:YLF regenerative amplifier which produces 50 ps pulses with an energy of 1.5 mJ at a 300 Hz repetition rate. The output of the regenerative amplifier is converted to second and fourth harmonics in a series of two BBO crystals. The 527 nm radiation remaining after the fourth harmonic crystal is used to pump a two-stage dye amplifier. The 263 nm pulse energy is limited to the 100–200 μJ range by detuning the fourth harmonic crystal away from optimum phase matching. Thus the amplified dye laser pulse energy is in the range of 10–15 μJ.

The 193 nm seed pulses are generated in another BBO crystal by mixing 263 and 724 nm pulses. Selecting a proper BBO crystal resulted in steady seed pulse energies of 1.5–4 μJ at 300 Hz. The seed pulses at 193 nm are amplified in a double pass ArF amplifier to an energy of 2–2.5 mJ, thus an average output power of 600–750 mW is obtained. Streak camera measurements of the amplified 193 nm pulses gave an upper limit of 9 ps [full width at half maximum (FWHM)] for the pulse duration.

Reliable operation of the system is critically dependent on the timing synchronization of the different components. The electronic components used for synchronization are also shown in Fig. 2. Given that this Nd:YLF regenerative amplifier possesses a different cavity round-trip time than the master cw mode-locked laser, the number of passes inside the regenerative amplifier must be fixed. The 38 MHz rf signal from the mode-locker of the master oscillator is used for timing the pulse selection and switchout signals for the Pockels cell in the regenerative amplifier, which then triggers a digital delay pulse generator. The delay generator becomes the central timing source for the ArF discharge, streak camera sweep, etc. A zero drift control module was used to limit the jitter in the gain timing of the excimer discharge to ± 2 ns. Such fluctuations of the discharge timing are tolerable given a seed pulse transit time through the amplifier of 7 ns and a discharge gain lifetime greater than 10 ns. Jitter in the amplifier timing affects the output pulse energy because of the nonuniform temporal gain profile typical of discharge-pumped excimer systems. The pulse-to-pulse intensity fluctuation under normal operating conditions depends on many factors, including gas lifetime and discharge parameters, but was typically less than 30% with a fresh gas fill. The ArF amplifier was equipped with a liquid nitrogen gas purifier which allowed up to 4 h operation with a single gas fill and less than 50% degradation of the output power at a fixed discharge high voltage. It is noteworthy to consider that at a 300 Hz repetition rate more than 10^6 pulses are amplified per hour. In this system picosecond pulses of several optical wavelengths (1053, 724, 527, 263, and 193 nm) are synchronized with the x-ray pulse to high accuracy (~ 10 ps).

IV. GENERATION OF PICOSECOND X-RAY PULSES

The output radiation from the ArF excimer amplifier was used to operate the x-ray diode (Fig. 1). Both the cathode and the anode were made from bulk samples of Al and Cu, respectively, and polished using Micro-Mesh® abrasives to achieve a surface roughness of less than 25 μm. The electrodes were cleaned with hexane and installed in the vacuum chamber. The flat surfaces of the anode (3 mm diameter) and cathode (12 mm diameter) were separated by 10 mm. The x-ray diode chamber was normally kept at pressure of $(4–7) \times 10^{-9}$ Torr. The UV radiation was directed on the cathode through a MgF_2 window at 15° relative to the normal of the cathode surface. The diode chamber was equipped with two 250 μm thick Be windows

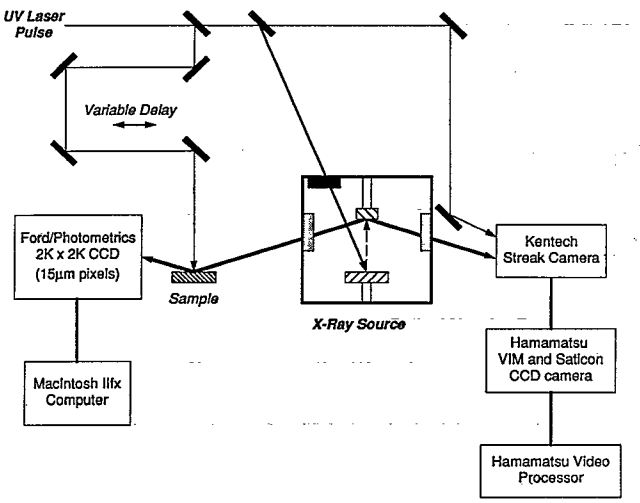

FIG. 3. Experimental setup for x-ray output diagnostics and picosecond time-resolved x-ray diffraction.

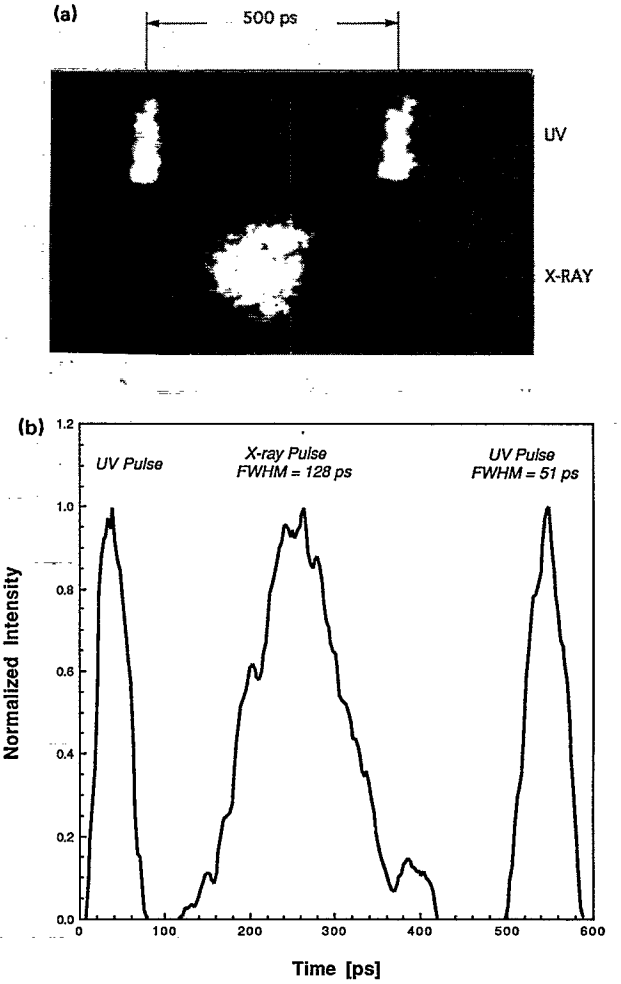

FIG. 4. (a) Streak camera data showing UV and x-ray pulsewidths accumulated in videoprocessor memory. (b) Scans of the UV and x-ray pulse images provide observed pulse durations of 51 and 128 ps (FWHM), respectively.

for the x-ray output (Fig. 3). One arm of the x-ray output illuminates a streak camera for timing and pulse duration measurements. The measured pulse duration of the amplified 193 nm pulse was 9 ps (FWHM), which is much less than the 190 ps electron transit time calculated for this x-ray diode.[13] Also, a repetition rate of 300 Hz implies a period of 3.3 ms between UV pulses so that the electron pulses in the diode do not overlap in time. Therefore the amount of Cu K_α x-ray photons produced by each UV pulse can be evaluated individually. At 70 kV anode–cathode voltage, the maximum amount of charge density which can be extracted from the cathode is 4.9×10^{-11} C/mm^2, which yields 3×10^8 electrons per pulse. Incorporating the efficiency of K_α production from a Cu target into the yield calculation[17] results in 3.7×10^5 photons of Cu K_α radiation being produced per unit solid angle per pulse.

Temporal measurement of the x-ray output was carried out with a high repetition rate, 3 ps resolution streak camera (Kentech Instruments Ltd.).[20] The photocathode of the camera was divided into two sections: a quartz window coated with 30 nm gold film sensitive to 193 nm radiation and 1.5 μm Mylar film coated with 30 nm thick low density CsI sensitive to x-ray photons. The streak camera output was optically coupled to a Hamamatsu Saticon charged coupled device (CCD) camera after amplification with an electrostatic image intensifier. The output of the CCD camera is stored on a Hamamatsu video processor for measurements and enhancement. Unfortunately, the x-ray output was insufficient for single shot measurements, and frame accumulation of several thousand shots was necessary to obtain a measurable signal. Two different trigger sources were employed to trigger the streak camera sweep: an additional channel from the same digital delay generator used to trigger the excimer amplifier, or the output of a fast vacuum photodiode illuminated by second harmonic pulses. Although in both cases successful measurements were performed, the jitter using the photodiode trigger was much less due to the reduction of the electronic jitter in the trigger circuit. An estimate of the effect of timing jitter on pulsewidth measurements must be included in an attempt to derive an actual pulsewidth from the streak camera observations. In order to estimate the jitter, the UV intensity incident on the streak camera slits was attenuated so that a UV pulse image was accumulated in the same number of frames ($\sim$2000) as a typical x-ray image. Figure 4(a) is a photograph of the streak camera image of two UV pulses separated by 500 ps and the x-ray pulse image from 2000 frames of integration. It should be noted that this image was deliberately overexposed to enhance the contrast for photographic reproduction. Scans of this image in the videoprocessor provide a measurement of the UV pulse duration of 51 ps (FWHM) as shown in Fig. 4(b). This figure also shows the x-ray pulse shape with an observed duration of 128 ps (FWHM). The amplified 193 nm pulsewidth is known to be less than 9 ps (FWHM) from previous measurements.[19] Scaling the x-ray measurement by the ratio of the known/observed UV pulsewidths in order to account for the effects of timing jitter gives a lower limit for the x-ray pulse duration of 20 ps. If the jitter broadens the observed pulse duration in a cumulative manner, then subtracting the difference of the UV pulsewidths from the

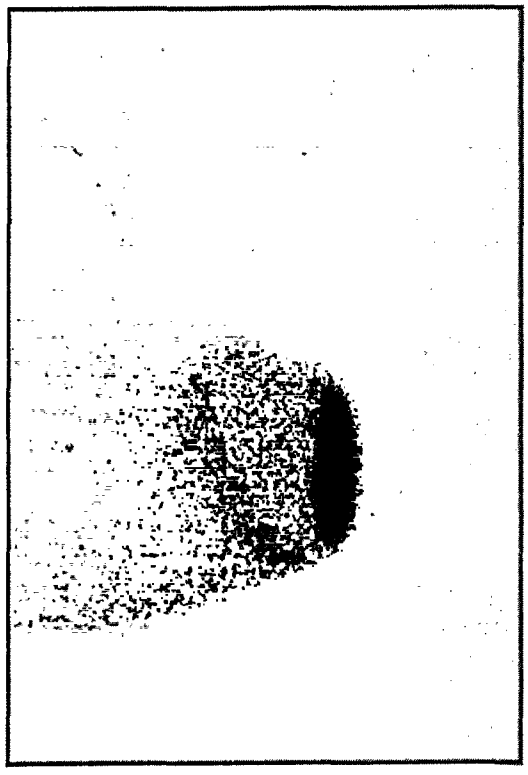

FIG. 5. X-ray pinhole picture of the anode.

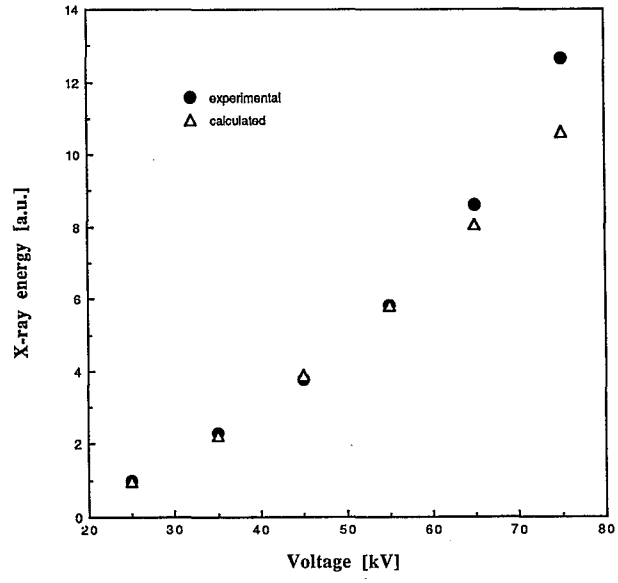

FIG. 6. X-ray energy as a function of the applied voltage.

observed x-ray signal may be a more appropriate adjustment that gives an upper limit for the x-ray pulsewidth of 90 ps. In any case, it is safe to assume the true x-ray pulse duration lies in the range of 20–90 ps. Using computer simulation data for the dispersion of short electron pulses across a diode in the space-charge regime, it is estimated that a 9 ps electron pulse at the cathode surface yields a 23 ps electron pulse at the anode.[14] This value is in agreement with the measured x-ray pulse duration, given the validity of the assumption that the x-ray pulsewidth equals the electron pulse duration at the anode.

The x-ray output from the diode through the other Be window was used to carry out spectral and time-resolved x-ray diffraction measurements. The UV beam from the excimer amplifier was attenuated and focused with 1 m focal length lens onto the cathode surface. The UV spot on the cathode was approximately 3 mm diameter and situated opposite the anode. No detailed study of the influence of the size and position of the UV beam on the cathode on the x-ray output was carried out. However, shifting the position of the UV spot on the cathode changed the distribution of the x-ray production from the anode surface. Pinhole pictures revealed that for the above positioning of the UV beam the predominant part of the x-ray output was generated on the flat surface of the anode. Figure 5 shows a pinhole image of the spatial x-ray distribution from the anode. It is noteworthy that the use of a photocathode allows, in principle, the implementation of more complicated geometries for varying the spatial and temporal distribution from the x-ray source.

The x-ray output was measured using a large area CCD camera designed specifically for direct x-ray imaging. The camera consists of a Ford Aerospace 2048×2048 MPP CCD chip (15 μm pixel), cooled by liquid nitrogen (Photometrics Ltd.), and interfaced to a Macintosh IIfx computer.[12] The active area of the CCD is 30×30 mm^2, and the conversion efficiency for 8 keV photons is about 15%. Cooling to low temperatures (-100 °C) reduces the dark current to allow for single photon detection. Camera readout at 50 kHz with 4×4 pixel binning was usually employed to increase the data acquisition rate, since the full 15 μm spatial resolution was seldom required.

The measured x-ray output flux at 40 cm from the anode and 10° takeoff angle was measured at 3×10^4 Cu K_α photons per cm^2 per second. This observed value was in good agreement with the calculated value for a pulsed x-ray diode with a saturated photocathode. Single or double crystal monochromator arrangements yielded ~3% Bragg reflection from a Si(111) crystal and about 6% Bragg reflection from a Pt(111) crystal. The measured ratio of intensities of the $K_{\alpha1}$, $K_{\alpha2}$, and K_β lines correspond to the output from a conventional x-ray tube.[21] Figure 6 shows the dependence of Cu K_α output on the applied voltage at constant UV illumination. The output increases slightly faster than $(V/V_K-1)^{1.67}$ due to the dependence of the available charge on the applied voltage (V_K represents the K-shell ionization voltage of the anode material).[21] When the x-ray diode was operated in the saturated mode the fluctuations of the x-ray output energy was found to be an order of magnitude less than the fluctuations in the input UV pulse energy. The estimated energy efficiency of this system for conversion of 193 nm radiation to Cu K_α radiation is approximately 0.5% of the UV flux necessary to saturate the x-ray photodiode.

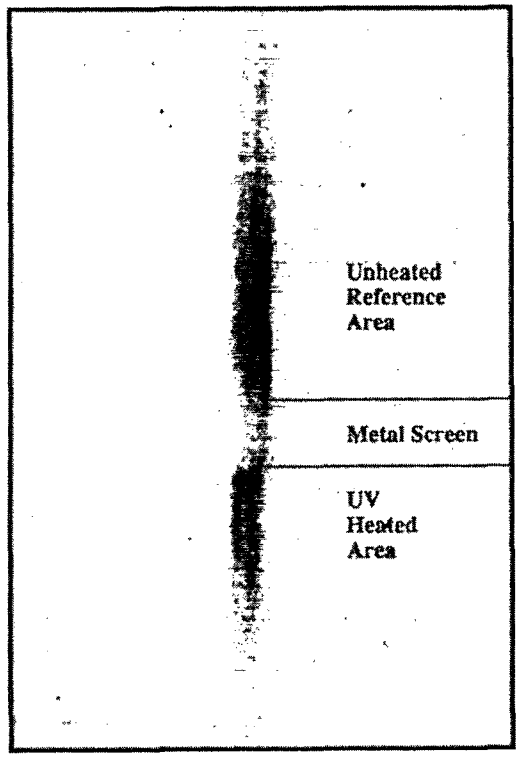

FIG. 7. CCD image of the diffracted x rays from the Pt(111) crystal. X-ray diffraction signals from unheated and heated parts of the crystal are separated by a metal screen.

V. PICOSECOND X-RAY DIFFRACTION

The output from the x-ray diode was used to perform for the first time picosecond time-resolved x-ray diffraction experiments. The goal of the experiment was to observe crystal lattice distortion due to picosecond light pulse heating. A platinum (111) crystal was placed on a three-axis Eulerian cradle at 50 cm from the anode of the x-ray diode. Two 0.5 mm parallel slits were mounted between the x-ray source and the Pt crystal to collimate the x-ray beam. The x-ray pulse impinged upon the sample at an angle of 19.87° (Bragg condition). The crystal dimensions (1 mm thick and 9 mm diameter) allow the CCD camera to record the diffracted x rays along the whole diameter of the crystal.

The output of the ArF amplifier was split in two arms, one used to drive the x-ray diode, and the other to heat the Pt crystal after a proper delay was inserted. The UV heating (pump) beam was focused on the crystal surface in a 2 mm diameter spot with approximately 1.5 mJ/cm^2 average energy density per pulse. Under such conditions no surface damage was observed even after many hours of irradiation. The timing between the heating pulse and the x-ray pulse was measured using the streak camera as discussed above.

Figure 7 shows a typical picture from the CCD detection system. With proper alignment the diffraction from the whole crystal is recorded. A metal screen positioned on the crystal surface divided the crystal into two segments, the lower section where the heating UV radiation was directed and an upper area not illuminated by the UV radiation during all measurements. The results reported here were produced by 30 min exposures (5.4×10^5 shots), and the signal from the upper part of the crystal was used as a reference in order to account for variations in the x-ray flux. Typically two consecutive exposures are made, one with UV radiation heating the lower part of the crystal, the next one without UV heating. Figure 8 is an example of the horizontal scan of such exposure averaging 20 pixels in the vertical direction (1.2 mm on CCD). Figure 8 depicts the reference signals (a) and (c), as well as the diffracted x-ray photons detected from the unheated (b) and heated (d) areas of the crystal. The decrease in intensity of the diffracted signal due to the heating is readily seen. The maximum decrease in the diffracted x-ray signal due to laser pulse heating was ~6% with the delay between the UV heating pulse and the probe x-ray pulse set at less than 100 ps. Within this experimental arrangement, the timing accuracy of the arrival of the pump and probe pulses at the sample was about 100 ps. When the delay of the x-ray pulse was increased to 400 ps relative to the maximum interaction, the diffracted signal decreased to 2%–3%, which was within the fluctuation of the measurements.

Temperature changes in the crystal due to laser heating affect the diffracted x ray by thermal strain which alters the lattice spacing and the thermal-ionic motion which decreases the scattering power (Debye–Waller effect).[22] These effects have been treated in detail only for a constant and homogeneous temperature distribution. A recent report[23] considering a short pulse laser heating on metals has shown that for 10 ps heating laser pulse the temperature distribution in the metal is temporally and spatially inhomogeneous. The penetration depth of the x-ray beam in the Pt sample is estimated to be about 600 nm compared to about 20 nm for the absorption length of the 193 nm radiation. Thus caution should be exercised when applying the standard expression for the estimation of the influence of the heating on diffracted x-ray signals. From these measurements we estimate that the temperature of the surface of the crystal was increased by 100–300 °C as a result of the picosecond laser pulse heating. More detailed measurements and discussion will be presented in a subsequent communication.

VI. CONCLUSION

A new type of short pulse x-ray source has been developed that is capable of generating high repetition rate hard x-ray pulses in the range of 10–100 ps. Replacement of the anode material allows a wide spectral range of characteristic wavelength to be generated. At 70 kV the estimated brilliance is about 300 kW/mm^2, which is several orders of magnitude higher than the conventional x-ray tube. However, in spite of the gain in peak power, the amount of K_α x-ray photons per pulse is too low for single shot time-resolved diffraction measurements. For most practical cases, accumulation of thousands of shots is necessary to produce reliable results. In order to preserve the picosecond time resolution of the measurements, low jitter between the x-ray probe pulse and the pump source must be maintained. As mentioned above, this system provides pi-

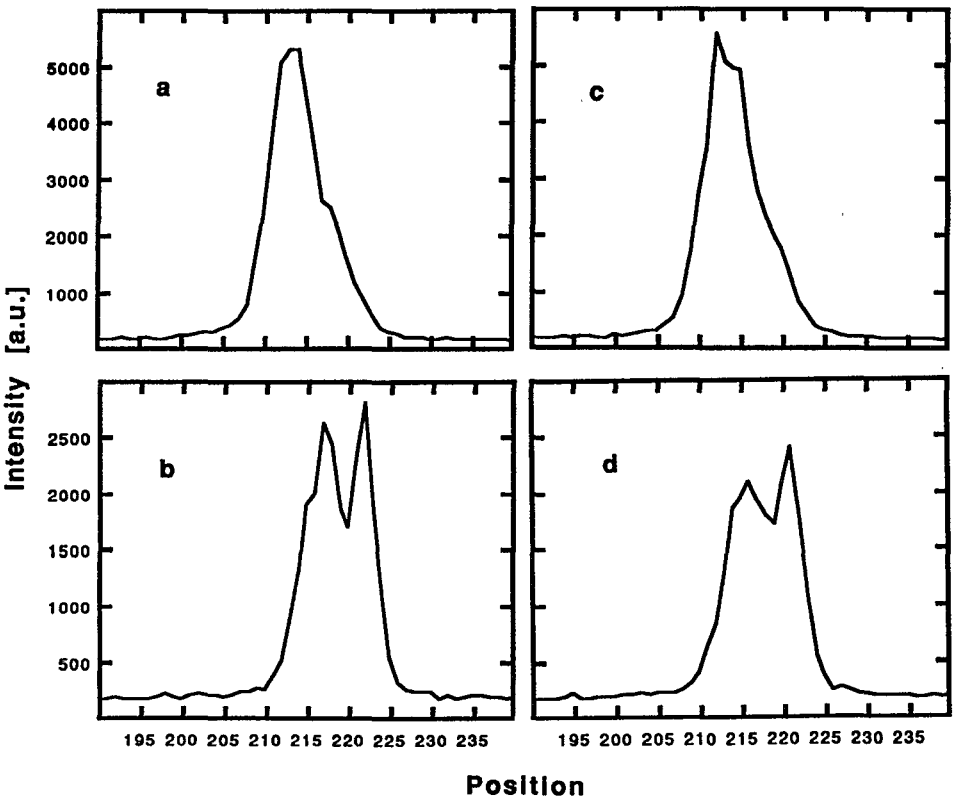

FIG. 8. Averaged pixel values of the diffracted x rays from two consecutive 30 min exposures. The signal strength is averaged over 20 pixels along the vertical axis and scanned along the horizontal axis of Fig. 7. The first exposure is without UV heating: (a) reference signal from unheated area and (b) diffracted intensity from the area where heating will take place. The second exposure when UV heating was applied: (c) reference signal from unheated area, and (d) diffracted intensity from the area of the crystal heated by the UV pump pulse.

cosecond pulses at several wavelengths which are accurately synchronized with the x-ray pulse; while for synchronization to other ultrafast phenomena, the rf signal of the cw mode-locked oscillator makes an excellent system clock. The observed jitter between the x-ray pulse and the output from the delay generator was approximately 200 ps using the rf signal as the trigger source (Fig. 2). This pulsed x-ray system has been used to observe a transient x-ray diffraction from a metal lattice on a picosecond time scale.

The low duty cycle of this system is determined by the 300 Hz repetition rate of the ArF excimer amplifier. Existing laser technology will allow the production of powerful UV pulses at repetition rates of several KHz with pulse durations in the picosecond and subpicosecond range, which may be exploited for further development of this technique for the generation of short x-ray pulses.

ACKNOWLEDGMENTS

This work was supported by the W. M. Keck Foundation and Defense Advanced Research Project Agency under AFOSR Contract No. F49620-089-C-0104.

[1] M. Yoshimitsu and S. Kozaki, Top. Appl. Phys. **22**, 9 (1977).
[2] R. Germer, J. Phys. E **12**, 336 (1979).
[3] J. G. Lunney, P. J. Dobson, J. D. Hares, S. D. Tabatabaei, and R. W. Eason, Opt. Commun. **58**, 269 (1986).
[4] B. C. Larson and J. Z. Tischler, SPIE Proc. **1345**, 90 (1990).
[5] B. C. Larson, J. Z. Tischler, and D. M. Mills, J. Mater. Res. **1**, 144 (1986).
[6] S. Kojima, I. Maekawa, S. Kawado, T. Takahashi, T. Ishikawa, and S. Kikuta, Rev. Sci. Instrum. **63**, 1164 (1992).
[7] N. Nakomo and H. Kuroda, Phys. Rev. A **35**, 4719 (1987); O. L. Landen, E. M. Campell, and M. D. Perry, Opt. Commun. **63**, 253 (1987).
[8] J. R. Bushchert, J. Z. Tischler, D. M. Mills, Q. Zhao, and R. Colella, J. Appl. Phys. **66**, 3523 (1989).
[9] B. G. Tenchov, H. Yao, and I. Hatta, Biophys. J. **56**, 757 (1989).
[10] J. Wong, E. M. Larson, J. B. Holt, and P. A. Waide, Science **249**, 1406 (1990).
[11] J. R. Schoonover and S. H. Lin, J. Solid State Chem. **76**, 143 (1988).
[12] B. Van Wonterghem and P. M. Rentzepis, SPIE Proc. **1204**, 784 (1990).
[13] J. P. Girardeau-Montaut and C. Girardeau-Montaut, J. Appl. Phys. **65**, 2889 (1989).
[14] C. Girardeau-Montaut and J. P. Girardeau-Montaut, Appl. Phys. Lett. **55**, 2556 (1989).
[15] T. Srinivasan-Rao, J. Fisher, and T. Tsang, J. Appl. Phys. **69**, 3291 (1991).
[16] T. Anderson, I. V. Tomov, and P. M. Rentzepis, J. Appl. Phys. **71**, 5161 (1992).
[17] M. Green and V. E. Cosslett, Proc. Phys. Soc. London **78**, 1206 (1961).
[18] C. E. Dick, A. C. Lucas, J. M. Motz, R. C. Placious, and J. H. Sparrow, J. Appl. Phys. **44**, 815 (1973).
[19] I. V. Tomov, T. Anderson, and P. M. Rentzepis, Appl. Phys. Lett. **61**, 1157 (1992); **61**, 3193(E) (1992).
[20] M. M. Murnane, H. C. Kapteyn, and R. W. Falcone, Appl. Phys. Lett. **56**, 1948 (1990).
[21] N. A. Dyson, *X-Ray in Atomic and Nuclear Physics* (Cambridge University Press, Cambridge, 1990).
[22] C. J. Hailey, G. Bush, R. Johnson, Z. Koenig, J. Lupton, R. Schroeder, D. Sullivan, and W. Goldstein, SPIE Proc. **690**, 19 (1986).
[23] T. Q. Qiu and C. L. Tien, Int. J. Heat Mass. Transfer **35**, 719 (1992).